Study of the ω phase in Zr-Nb alloys by Mössbauer and x-ray diffuse scattering

W. Lin,* H. Spalt,† and B. W. Batterman
Department of Materials Science and Engineering and School of Applied and Engineering Physics, Cornell University, Ithaca, New York 14853
(Received 6 October 1975)

The ω phase transformation in Zr-Nb alloys has been studied by measuring x-ray and Mössbauer diffuse scattering from single crystals with compositions ranging from 8- to 30-wt% Nb. We present an extensive two-dimensional mapping of the x-ray diffuse scatttering for all compositions. The distinct features of these experimental observations are (a) the x-ray ω reflections are displaced, in general, toward a lower angle from the hexagonal positions, (b) the Mössbauer elastic scattering is shifted toward a lower angle while the inelastic portions are centered at the exact hexagonal positions. Our intensity calculations indicate that no single model, based either on an independent-particle approach or a wave model, accounts for the observed scattering features. The displacement of x-ray peaks seems to be consistent with two effects: a phononlike distortion with a wave vector k_m slightly larger than k_ω (the exact value) and a Bain-type lattice expansion. A possible mechanism behind the Mössbauer elastic peak shifts is presented based on energetic considerations. The metastable athermal ω may be viewed as the result of time-dependent fluctuations of the bcc lattice into ω-like regions. The size and time dependences are strongly composition dependent. At 15-wt% Nb and lower, ω regions are quite large and long lived, and they are essentially crystalline in nature. At high concentrations, the ω domain fluctuations are small and short lived.

I. INTRODUCTION

There has been considerable interest in recent years in certain alloys of Zr and Ti with elements such as V, Nb, and Ta (group V*B*) and Cr and Mo (group VI*B*). Much of the interest was generated because of the appearance of a metastable low-temperature phase, called the omega (ω) phase which hinted strongly of lattice instabilities and soft modes. Its formation is generally thought to be representative of a more fundamental instability of bcc with respect to hcp. The basic structural investigations were made by Silcock, Davies, and Hardy[1] and have been extended by several other workers.[2-5]

At high temperatures the alloy is a bcc solid solution which, upon quenching, retains an average bcc structure with a marked instability to the formation of the so-called ω phase. This athermal ω phase is in general trigonal. The amount of ω relative to the bcc phase, the degree of crystallinity and size of the ω regions are strongly dependent on Nb concentrations.

Recent x-ray[5] and electron diffraction investigations by Dawson and Sass[6] show that at concentrations between 5-wt% and about 17-wt% Nb, reasonably sharp athermal ω Bragg reflections appear, while for concentrations between 17- and 30-wt% Nb diffuse scattering occurs in the vicinity of the sharper lower concentration ω reflections. In general the higher the Nb concentration the greater the tendency to suppress any transformation out of the bcc phase.

The athermal ω phase can be described as resulting from bcc, by translation of pairs of $\{111\}$ planes in $\langle 111\rangle$ directions in an ordered way.[3,7] Using a phonon description, the displacements due to a static longitudinal phonon of wavelength $3d_{222}$ (usual notation $\frac{1}{2}[111]$) would transform bcc into ω, where d_{222} is the bcc (222) interplanar spacing. One can describe the bcc sequence in the $\langle 111\rangle$ direction as $ABCA\ldots$, where the A-A separation is the near-neighbor spacing in bcc. The transformation is then simply the collapse of the BC planes toward their midplane with the A-A spacing remaining unchanged. Full collapse of the BC planes to their midplane would result in an hexagonal structure whereas for partial collapse it is trigonal. The crystallography is concisely reviewed by Keating and LaPlaca.[8]

The present work was initiated to provide a thorough experimental investigation of the nature of the ω-phase diffuse scattering in Zr-Nb as a function of Nb concentration and to use the Mössbauer technique to separate the scattering into its elastic and dynamic components.

It is useful to review some recent work to put things in perspective. Sass's[7] electron-diffraction results showed several interesting features. We show in Fig. 1 his results as a function of composition for Zr-Nb. It is clearly evident that the scattering becomes more diffuse as Nb concentration is increased. Further as can be seen in Fig. 1(d) the diffuse scattering is displaced from the exact ω-phase positions. For example if we consider the $\langle 111\rangle_\beta$ ($\langle 00\cdot 1\rangle_\omega$) direction we see that the (00·1) and (00◦4) diffuse peaks are displaced away from the origin of k space while the (00·2)

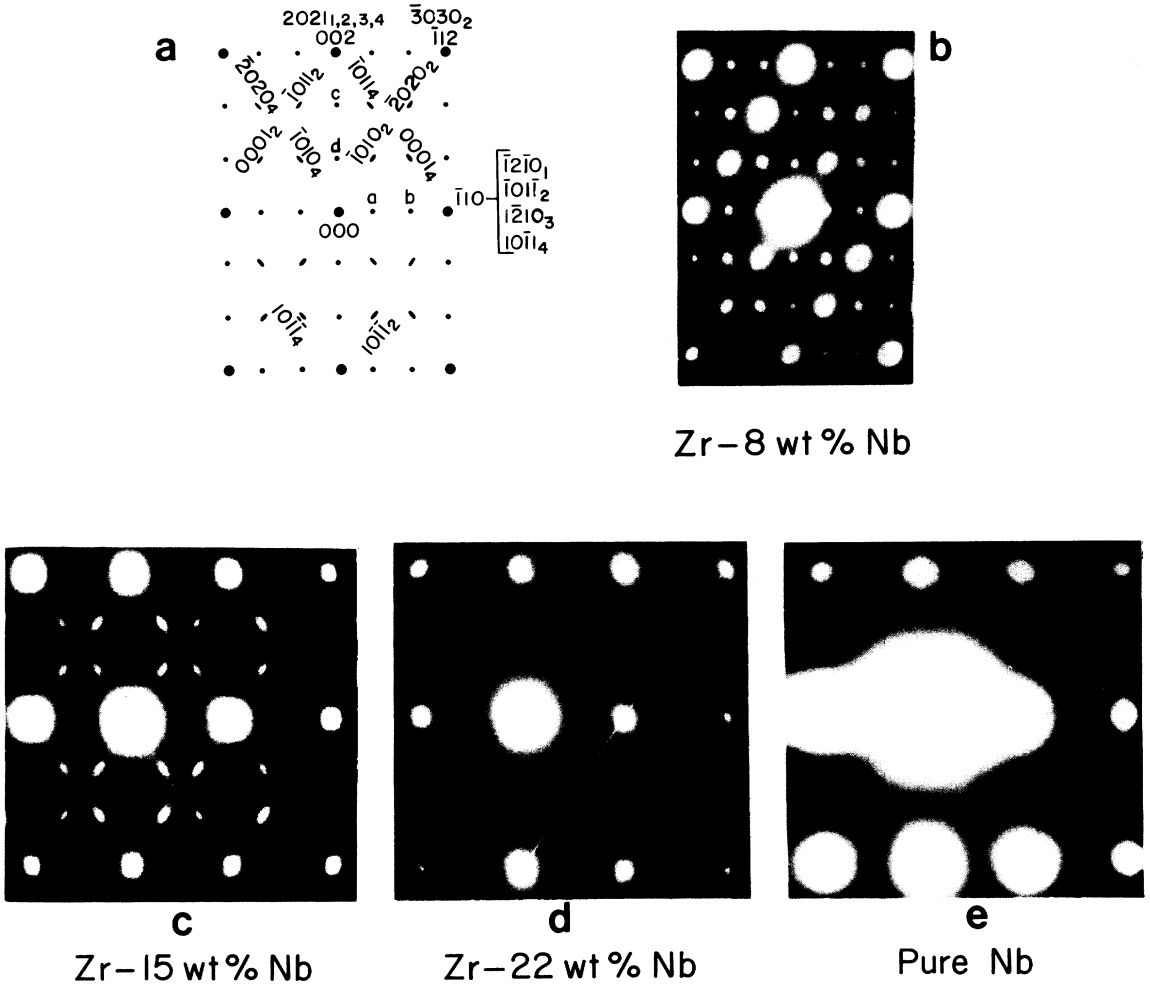

FIG. 1. Comparison of (110) electron diffraction patterns of several Zr-Nb alloys (from Sass, Ref. 7). (a) Schematic diffraction pattern giving indices of the reflections shown in (b)–(e). The subscripts refer to orientations of the ω phase with respect to the four different [111] directions (variants). (b) 8-wt% Nb, (c) 15-wt% Nb, (d) 22-wt% Nb, (e) pure Nb.

and presumably the (00·5) are displaced in the opposite direction. A serious limitation of this electron diffraction study is the appearance of diffuse peaks due to multiple scattering. Keating and LaPlaca[8] measured the diffuse scattering of neutrons in the (110) bcc reciprocal-lattice plane of a $Zr_{0.8}Nb_{0.2}$ alloy. A striking difference between the electron and neutron diffraction patterns is that the (00·4) diffuse reflection is absent in the latter. Furthermore, the intensities of the (10·3) and ($\bar{1}$0·3) are quite different in the neutron results whereas they appear to be of equal intensity in the electron diffraction pattern. Also clear in their plot is the existence of extra diffuse scattering in the vicinity of the allowed bcc reflections.

In a subsidiary work Moss, Keating, and Axe[9] using high-resolution inelastic-neutron-scattering techniques ascertained that the diffuse scattering at an ω position (10·1) was elastic to about 10^{-6} eV. At this point using a Mössbauer technique to be described in this paper, Batterman, Maracci, Merlini, and Pace[10] showed that the diffuse scattering has a substantial inelastic fraction, which increases with increasing diffraction vector.

In a further work Moss, Keating, and Axe[11] showed that the elastic central peaks persisted [for the ($\bar{1}$0·3) reflection] to 1273 °K, well into the single-phase β region. This rather remarkable result implies a static ω-like structure even at these high temperatures. In both these works, i.e., Refs. 9 and 11, it appears in hindsight that there is a non-negligible inelastic portion to the scattering at the ω positions when one includes scattering shifted as much as 2×10^{-2} eV (20 meV).

Borie *et al.*[12] devised an *ad hoc* model that matched many aspects of the observed neutron results presented by Keating and co-workers. Their model consisted of a fully transformed ω structure taking into account that the fixed bcc plane in the ω transformation can be planes B and C as well as A in our description above. Within the bcc reference system, ω regions based on invariant A, B, or C planes are called subvariants. Borie *et al.*[12] treat the ω phase as made up of sequences of small subvariant regions and find that only certain sequences of subvariants will reproduce the sense of the experimentally observed shifts of the diffuse peaks. We will come back to this point in the discussion section. Borie's model does not predict any diffuse scattering around the bcc positions.

In order to help gain a more fundamental understanding of the ω-phase formation we have made a systematic study of a range of Zr-Nb alloys. We have measured both the x-ray and Mössbauer diffuse scattering from samples containing 8-, 12-, 15-, 20-, and 30-wt% Nb.

II. EXPERIMENTAL PROCEDURE

A. X ray

Large single crystals of Zr-Nb alloys were cut into disks of about 1 cm diameter and 3 mm thick and slabs $1\times2\times0.3$ cm^3 with (111) faces. These crystals were metallographically polished and chemically etched to remove surface damage and strain.[13]

The x-ray diffuse scattering measurements[14] were made using Mo $K\alpha$ radiation monochromated by diffraction from a doubly bent LiF crystal of the Warren-Chipman type.[15] The scattered radiation was detected with a NaI (Tl-doped) scintillation detector equipped with a single-channel pulse-height analyzer. The divergence in primary and scattered beams was restricted by slits to 0.5° in the horizontal and 1.4° in vertical directions as measured by the (555) reflection of a perfect silicon crystal. The resulting resolution volume is shown in the insert of Fig. 2. A modified General Electric three-axis diffractometer was automated and controlled by a PDP-8/e computer through interfaced stepping motors which drive 2θ (counter angle), χ (crystal tilt in a plane normal to the plane of incidence and containing the diffraction vector), and ϕ rotation about the $\langle 111\rangle$ axis of the crystal.

All experimental data were stored and processed using a PDP-12 computer equipped with magnetic tapes, disk storage, and plotters. A series of programs were developed for various corrections,

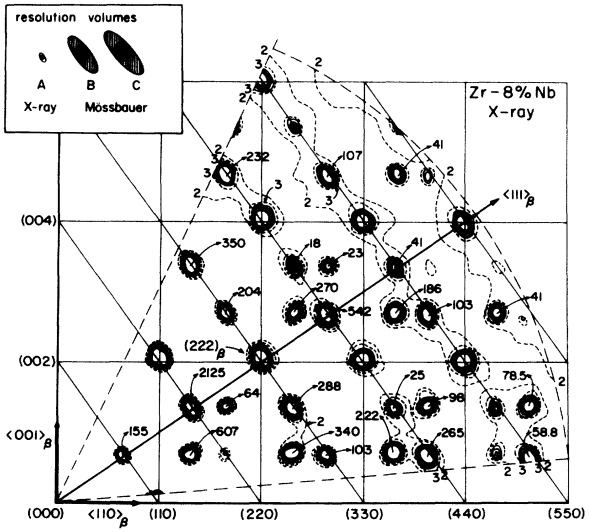

FIG. 2. Zr–8-wt% Nb. Contour map of x-ray scattering in the $(1\bar{1}0)$ bcc reciprocal-lattice plane. The contours represent 2, 3, 5, 7, 9, 11, 13 times 2.5 electron units per atom divided by f_{av}^2. The peak intensities of the individual ω reflections when greater than the level 13 are directly given in the same contour units. In the insert, A is the resolution volume used in the x-ray measurements. The singly-hatched area is the section of the resolution volume in the plane of the figure, and the small cross-hatched area is the section normal to the figure. The outer contour corresponds to a level $\frac{1}{5}$ of the maximum. Inserts B and C are the corresponding volume elements used in the Mössbauer scattering experiments.

conversions and contour map plotting using an analog recorder equipped with a point-plot pen.

The primary beam intensity was monitored using the scattering from a block of polystyrene $(C_8H_8)_x$ at an angle of $2\theta=41.6°$ ($\sin\theta/\lambda=0.5$ Å^{-1}) before and after each experimental run. Primary beam stability was also checked periodically in reciprocal space of the crystal.

The scattered intensities were converted to absolute units (electron units per atom) by determining the primary beam intensity. This was obtained from a measurement of the integrated intensities of (111) or (200) reflections from an aluminum-powder sample,[16] using the same experimental conditions as with the diffuse scattering determination. From the experimental value for the absolute integrated intensity taken from Ref. 16 and the measured integrated powder intensities, the direct beam could be determined.

The resolution of the scintillation detector did not allow for electronic discrimination of the Zr and Nb K fluorescence produced by the primary Mo K_α radiation. To determine this contribution we used a solid state detector with sufficient resolution to separate the various wavelengths.

We recorded the scattering from the specimen in a low-intensity region ($\sin\theta/\lambda = 0.9$ Å^{-1} in a $\langle 111 \rangle$ direction). At this point about 12% of the total scattering was due to fluorescence. This fluorescence was measured as certain fraction of the incident power, and could then be used to correct all data for that particular crystal.

The contribution to the scattering due to the half-wavelength component of the radiation passed by the monochromator was checked and was found insignificant at all scattering angles.

B. Mössbauer

The principle of the Mössbauer experiment is described in detail elsewhere.[17] An experimental set up similar to that of Batterman *et al.*[10] was used. The source, ^{57}Co diffused into a chromium platelet, had an active area of 6×6 mm^2 and a nominal activity of 200 mCi. The absorber was a stainless-steel foil, 98% enriched in ^{57}Fe, with a thickness of 1 mg/cm^2. This combination of source and absorber is very close to the maximum of the nuclear resonance absorption when both are at rest. The fraction of the recoilless γ quanta to the total number of 14.4-keV quanta was found to be $\rho_0 = 0.62$. This value was checked periodically and minor changes were taken into account.

In order to separate the elastic and inelastic intensity contributions, Mössbauer γ rays were measured with and without a resonant absorber between sample and detector. That portion of the γ rays scattered inelastically, losing energies greater than the Mössbauer resonance width ($\pm 2\times10^{-8}$ eV), will undergo significantly smaller attenuation in the resonance absorber than the elastic portion.

Associated with the 14.4-keV nuclear transition are 120- and 136-keV γ-ray lines. These high-energy γ rays can contribute to the count rate in the 14.4-keV channel. By placing an aluminum absorber between the source and sample (thick enough to completely absorb the 14.4-keV line) a correction can be determined to eliminate contributions from these high-energy γ-ray lines.

A significant improvement in the present set up compared to that described in Ref. 10 is the fact that the scintillation counter was replaced by a moderately high-energy resolution solid-state detector. The lithium-drifted silicon detector had a resolution of 338 eV [full width at half-maximum (FWHM)] at 14.4 keV. The use of this counter enabled us to electronically discriminate against the fluorescence of Nb and Zr excited by the high-energy γ rays. Thus we avoided the use of a RbCl filter (necessary in earlier work) which cut down the total intensity by a factor of approximately 2. Furthermore, the intensity measured with the aluminum filter was the same to within 1% with the Mössbauer absorber, either in or out. Therefore, only three instead of four measurements had to be made at one angular setting. Because of the narrow bandwidth of the solid-state detector the scattering associated with the 120- and 136-keV γ rays was a factor of 7.5 weaker than that measured with a scintillation counter, thus significantly improving the signal-to-noise ratio. The net effect of the solid-state detector was to decrease our counting time for a given precision by roughly a factor of the order of 10 over the previous setup.

III. EXPERIMENTAL OBSERVATIONS

A. X ray

Diffuse x-ray scattering was measured for single crystals of Zr-Nb alloys containing 8-, 12-, 15-, 20-, and 30-wt% Nb. These crystals were heat treated at 1000 °C in the β-phase region and then quenched into room-temperature oil. Figures 2–6 show the measured diffuse intensity distribution in $(1\bar{1}0)$ plane of the bcc reciprocal space. The measured region includes the $\langle 111 \rangle$ axis and extends to $\sin\theta/\lambda = 1$ Å^{-1}. The intersections of the rectangular grid lines represent the bcc reflections. Before discussing the details of the diffuse scattering measurements, consideration of a schematic of this $(1\bar{1}0)$ plane shown in Fig. 7 would be helpful. We show here the relationship between reflections of the bcc and hexagonal phases. The ω particles which form with equal probability along any of the four $\langle 111 \rangle$ crystallographic axes of the β structure are referred to as four ω variants. For a given $(1\bar{1}0)$ plane, there are two $\langle 111 \rangle$ axes contained in the plane with an angle of 70.5° be-

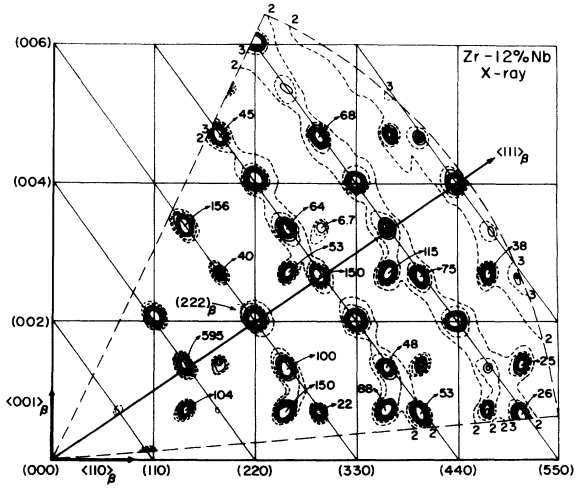

FIG. 3. Zr–12-wt% Nb. Otherwise same as Fig. 2.

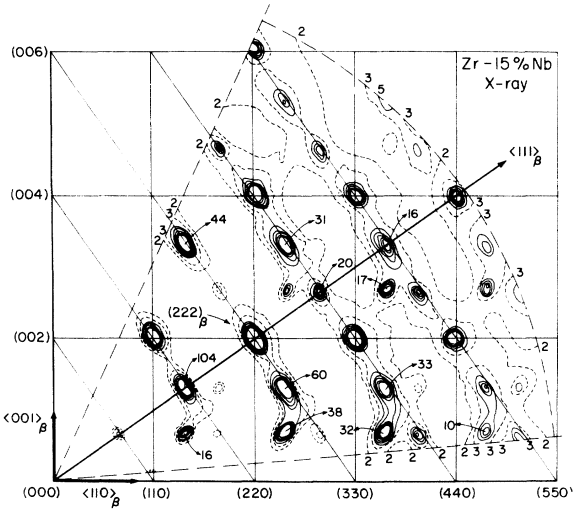

FIG. 4. Zr–15-wt% Nb. Otherwise same as Fig. 2.

tween them, corresponding to variants 1 and 3 or variants 2 and 4. In the present case, we arbitrarily call the ω particles along [111] and [$\bar{1}\bar{1}$1] variants 1 and 3, respectively. Only these two ω variants contribute hexagonal reflections at non-bcc recriprocal-lattice points. However, each bcc lattice point is also the position for ω reflections from all four variants. Thus, reflections due to one ω variant occur on the lattice lines perpendicular to a $\langle 111\rangle_\beta$ axis, along which the corresponding ω particles are propagated. We have labelled these layer lines l_1 and l_3 to indicate those belonging to the ω_1 and ω_3 variants. Note that all ω reflections along lines $l_1 = 0$ and $l_3 = 0$ have no contribution in the $(1\bar{1}0)$ plane because the phase factor for the displacement $\bar{k}\cdot\bar{r}$ is zero for each respective variant along these layer lines.

The intensity distributions shown in Figs. 2–6

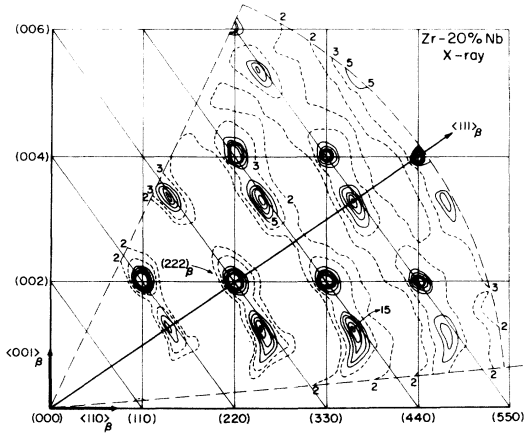

FIG. 5. Zr–20-wt% Nb. Otherwise same as Fig. 2.

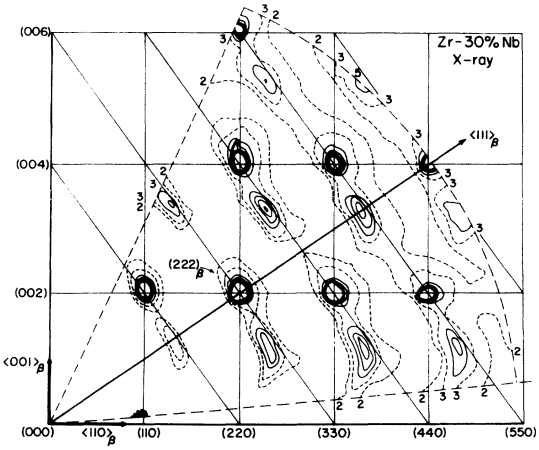

FIG. 6. Zr–30-wt% Nb. Otherwise same as Fig. 2.

are in absolute units and are corrected for the angular dependence of atomic scattering factors and polarization factors. The Compton scattering and fluorescence have also been removed. The same intensity levels and increments are used in all contour maps in Figs. 2–6 and thus they can be directly compared.

The intensity distribution from the Zr–8-wt%-Nb alloy in Fig. 2 shows very little diffuse intensity. The ω reflections are nearly as sharp as bcc reflections. All ω reflections occur at, or nearly at the calculated hexagonal lattice points. As the solute concentration increases, the formation of this highly crystalline ω phase is suppressed and the transformed structure deviates further from hexagonal. As a result, the diffraction pattern be-

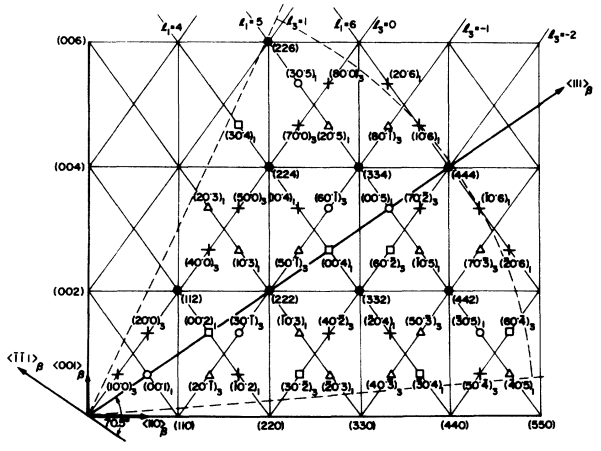

FIG. 7. Schematic of $(1\bar{1}0)$ bcc reciprocal-lattice plane giving indices of hexagonal ω reflections with subscripts referring to the different ω variants. Symbols □, △, ○, + represent the magnitude of the square of the geometrical structure factor of the ideal ω cell and are 9, 4, 1, 0, respectively.

comes more diffuse as can be readily seen by comparing Figs. 3–6. As the Nb content reaches 20 and 30-wt%, no sharp ω reflections are observed. Present are only broad, diffuse regions localized in the vicinity of the hexagonal positions as well as in the vicinity of the bcc matrix reflections. For example, the peak intensity of $(00\cdot2)_\omega$ for 20-wt% Nb is more than 10 times weaker than that of the corresponding peak in 15-wt%-Nb sample. Furthermore, note that some ω reflections, which are quite strong for low Nb concentrations, are very weak or undetectable in the 20- and 30-wt% samples. No reflections due to variant 3 are observed in the 20- and 30-wt% samples except for some weak vestiges in the vicinity of the $(30\cdot\bar{2})$ and $(40\cdot\bar{3})$ ω reflections. Note in particular the complete absence of the $(00\cdot4)$ reflection in Fig. 5 and 6, whereas it is quite strong for all the other concentrations.

Also to be noted is the change in shape of the ω reflections as Nb concentration increases. The diffuse regions tend to elongate perpendicular to $\langle111\rangle_\beta$-type axes. This is indicative of rod-shaped ω domains with their long dimension parallel to $\langle111\rangle_\beta$ axes. By examining the line profiles of the ω reflections, the width (FWHM) gives an estimate of the average size of coherently diffracting ω domains. For our purposes it can be assumed that the instrumental broadening function is negligible. From the profiles along the $\langle111\rangle_\beta$ axis we can get a rough idea of the long dimension of the rodlike domains. We obtain 60, 40, and 20 Å for the 8-, 15-, and 20-wt% Nb crystals, respectively. This is in good agreement with Keating and LaPlaca's[8] value of 23 Å for the 20-wt% alloys.

The diffuse intensity distribution characteristic of the ω phase in Zr-Nb alloys appears to be divided into two distinct categories; those for 8-, 12-, and 15-wt%-Nb crystals have rather similar patterns while the more broad and diffuse patterns from 20–30-wt% Nb are almost identical to one another except that the 20-wt%-Nb crystal exhibits peak intensities (10–15)% higher than the 30-wt%-Nb crystal. The other important and obvious features are the shifts (towards the origin) of the intensity maxima of the ω reflections away from the hexagonal positions. In the lowest Nb concentration alloy investigated, 8-wt% Nb, we can hardly notice any shift. The shift becomes more significant as Nb content increases and the ω peaks broaden. The effect is most pronounced for the 20- and 30-wt%-Nb crystals. Careful measurements show that the shift is parallel to $\langle111\rangle$ direction, not along the radial direction passing through the origin of reciprocal space. Peak shifts in Zr-Nb have been observed in electron diffraction patterns[7] and were characterized as follows: The ω peaks shift along lines parallel to various $\langle111\rangle$ directions and the shift is away from the nearby bcc lattice points [Brillouin-zone centers]. For example, the $(00\cdot4)_\omega$ and $(00\cdot5)_\omega$ diffuse maxima are shifted towards one another and away from $(222)_\beta$ and $(444)_\beta$, respectively. The $(00\cdot1)_\omega$ and $(00\cdot2)_\omega$ shift in a similar manner.

The present x-ray measurements indicate a rather different aspect with respect to the peak shifts. All peak shifts, except for $(00\cdot1)_\omega$, were found to be in the sense towards the origin as is apparent from the diffuse maps in Figs. 4–6. These findings have been confirmed by careful radial scans as well as some detailed localized intensity distribution measurements where the ω peaks are compared to bcc Bragg peaks along the same $[00\cdot l]$ layer line. The present Mössbauer scattering experiments also indicate the same type of peak-shift, as will be discussed in Sec. III B. For 20- and 30-wt%-Nb alloys, $(00\cdot1)_\omega$ is observed to be shifted away from the origin. This is not shown in the maps since the intensity is lower than the levels used in the contour maps. No $(00\cdot1)_\omega$ shifts were detectable in the alloys with lower Nb contents. For accurate determination of the peak position we used direct film mapping of the reciprocal lattice using a precession camera and a small single crystal of 15-wt% Nb rotating about its $\langle111\rangle$ axis. Within the optical measurement error no shift was detected for $(00\cdot1)_\omega$.

The amount and sign of the peak maxima shifts from their associated hexagonal positions cannot be described by any one model such as the soft phonon idea of deFontaine *et al.*[18] and Sass *et al.*[19] This model predicts shifts of ω peaks away from the bcc Brillouin-zone centers corresponding to a fixed $|\Delta K|$ in each. This is not consistent with observation.

The intensities of the Bragg reflections are not considered in this paper (an extensive neutron study of the Bragg peaks on the 20-wt%-Nb alloy has been given by Keating and LaPlaca[8]). It may however be noted that the diffuse scattering under the bcc reflections are almost the same for all reflections and decrease very slightly with increasing k vector. This is an indication that the scattering is rather of the type of particle size broadening than strain induced, because in the latter case the broadening should increase roughly as k^2.

B. Mössbauer

Mössbauer data were taken in radial runs along the $\langle111\rangle$ directions of the same crystals as used in the x-ray experiments. The results are shown in Figs. 8–11 for various compositions. Intensi-

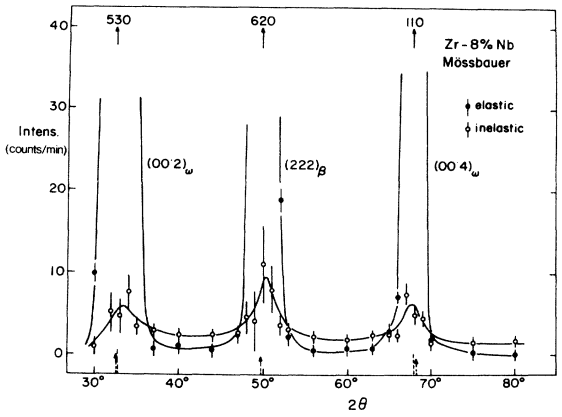

FIG. 8. Zr–8-wt% Nb. Elastic and inelastic Mössbauer scattering along the ⟨111⟩ direction vs scattering angle 2θ. The two dotted lines on the 2θ scale show expected and observed ω peak positions. The line with an arrow indicates the exact hexagonal position. The other line shows the observed position for the elastic peak. Peak intensities are given numerically at the top of the figure. Unless otherwise indicated all Mössbauer data are taken with resolution volume B in Fig. 2.

ties in counts/min are plotted versus scattering angle 2θ. Elastic scattering (full circles) and inelastic scattering (open circles) were separated using the ^{57}Fe absorber as described in the experimental section. Since the data were corrected for electronic and cosmic background only, the inelastic portion includes all inelastic scattering, i.e., Compton scattering and thermal diffuse scattering. The observed peak positions of the elastic scattering are indicated by dashed vertical lines. The calculated positions of the ideal hexagonal reflections are indicated by arrows on the abscissa.

At 8-wt%-Nb concentration (Fig. 8) the reflections are very sharp, in agreement with the x-ray results and the inelastic scattering is very weak compared to the elastic. No peak shifts are observed. As the Nb concentration increases, the

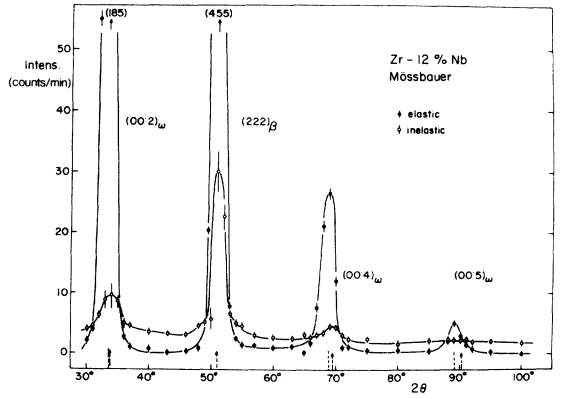

FIG. 9. Zr–12-wt% Nb. Otherwise same as Fig. 8.

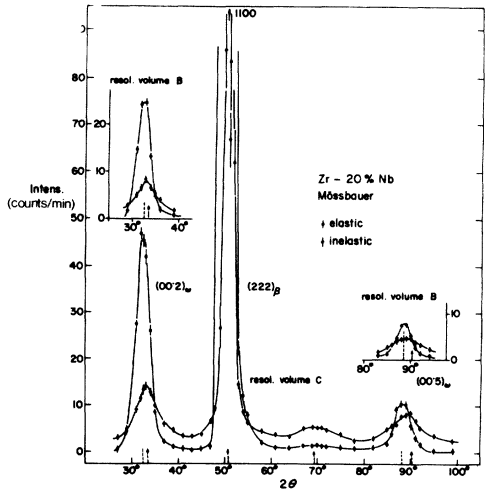

FIG. 10. Zr–20-wt% Nb. Otherwise same as Fig. 8. The complete curve is shown for the larger volume element C (Fig. 2). For comparison we show in the two inserts the ω peaks for the smaller volume element B.

elastic portions of the ω reflections clearly decrease. An extreme case of this is the $(00\cdot4)$ reflection which is virtually zero for the 20- and 30-wt% crystals. Note also that the inelastic scattering behaves in the opposite sense with increasing Nb concentration.

The actual scattered intensities unfortunately cannot be quantitatively compared for the different compositions. Some of the crystals were considerably smaller than the illuminated area at the sample position, (particularly the 8 and 15 wt% and to a lesser extent 12 wt%). The 20- and 30-wt% samples were large enough to intercept the entire beam. We show in Fig. 12 the inelastic/elastic intensity ratio as a function of composition for several ω reflections. The results suggest that there are two regimes in the athermal ω formation, one

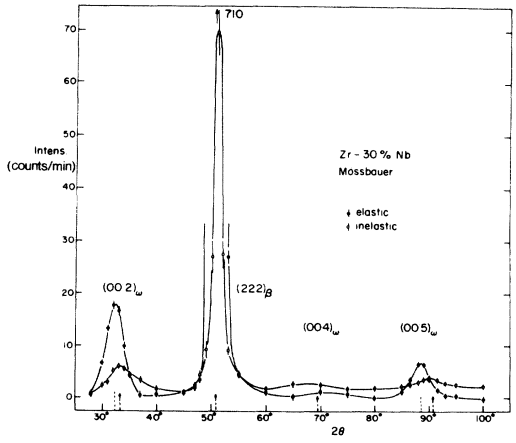

FIG. 11. Zr–30-wt% Nb. Otherwise same as Fig. 8.

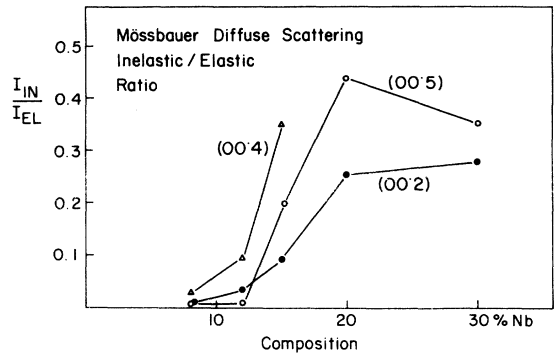

FIG. 12. Mössbauer inelastic-elastic ratio vs composition for various ω reflections.

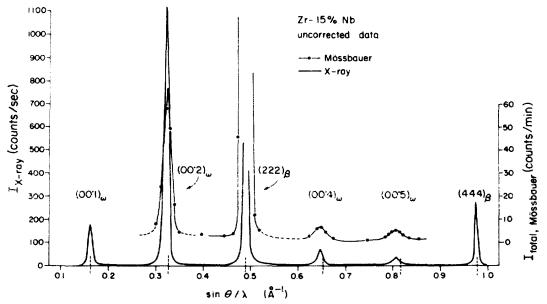

FIG. 13. Zr–15-wt% Nb. Uncorrected count rates of x-ray and total Mössbauer scattering ($I_{el} + I_{in}$) along the $\langle 111\rangle_\beta$ direction. On the abscissa are shown the exact hexagonal peak positions.

at low the other at high concentrations of Nb. The transition region is around the 15-wt% concentration.

Note the peculiar behavior of the inelastic scattering at the $(222)_\beta$ bcc reflection. At 8 wt% this inelastic portion is very small compared to the elastic. As we progress towards 30 wt% the inelastic peak increases by almost a factor of 3.5 (this is corrected for sample size differences). In the 8-wt% alloy this inelastic scattering is most probably mainly due to thermal diffuse scattering (TDS). The long-wavelength elastic constants[20] do do not change markedly in this composition range and therefore the thermal diffuse scattering should not change much between 8- and 30-wt% Nb. (Actually the elastic constants increase slightly with increasing Nb concentration. Therefore, if any change in thermal diffuse scattering should occur, it should be a decrease for higher compositions.) Thus, we can conclude that the inelastic scattering at the bcc Bragg reflections is most probably due to the large inelastic portions of the ω peaks which are coincident with the bcc matrix reflections.

One rather remarkable aspect of the scattering is the relative peak positions of the elastic and inelastic portions of the ω scattering as composition is changed. We see by comparing Figs. 8–11 that the inelastic portion always peaks within experimental error at the exact ω hexagonal lattice positions. As Nb concentration increases, the *elastic* portion of the (00·2) and (00·5) shifts further and further from this exact position towards the origin. This shift for a given composition increases for peaks further out in k space. We carefully checked to make sure that the peak shift of the elastic portion is not due to a peculiarity in our resolution volume. We measured the (00·2) and (00·5) peaks of the 30-wt%-Nb crystal using a resolution volume reduced in the $(1\bar{1}0)$ plane to about 60 wt% of the resolution volume B. The size perpendicular to the $(1\bar{1}0)$ plane was about the same. We found that the peak shifts were still present in both cases. At first sight the shifts of the x-ray and elastic Mössbauer peaks are not consistent with one another. However, if we realize that the x-ray scattering consists of both shifted elastic and unshifted inelastic contributions the situation becomes clear. To check this we plotted the total Mössbauer scattering ($I_{el} + I_{in}$) and compared it with the x-ray scattering for a run in the $\langle 111\rangle_\beta$ direction. In Fig. 13 we find excellent agreement between both measurements. The differences in the peak widths are due to the different sizes of the resolution volumes.

These Mössbauer results give some insight into a puzzling observation by Keating and LaPlaca.[8] They measured the Bragg intensities of many bcc reflections in a Zr–20-wt%-Nb sample and deduced from a model both static and thermal Debye parameters. They calculated the intensity of the ω diffuse reflections based on an ω structure with a given displacement parameter to which they added both static and thermal Debye factors. The best fit to observation was obtained when the calculation ignored both the static and thermal Debye-Waller factors. From our observations, the inelastic portion of the ω scattering is concentrated at the ω positions. Since this inelastic scattering represents both thermal and slow displacive motions (which look like static displacements to Bragg reflections) the total scattering at the ω positions as measured by a nonenergy selective technique corresponds to the pseudostatic arrangement of atoms. In other works, the static Fe^{-M} plus the diffuse $F(1 - e^{-M})$ contribute in the same region of k space so the net ω scattering should go as F, the nominal static value.

IV. DISCUSSION OF RESULTS

The scattering results presented in this paper pose several new and interesting questions re-

lated to the nature of the ω-phase transformation. It was previously accepted that the ω diffuse peaks were all symmetrically displaced away from the Brillouin-zone (BZ) center and were thus describable by a displacive $\langle 111 \rangle$ wave vector k_m somewhat greater than k_ω corresponding to the exact ω-phase position. Except for the $(00 \cdot 1)$ ω peak, the experimental results show that a displacement of all diffuse peaks in one direction is in fact correct and that symmetrical displacement about the BZ center is not the case. [For example, see the conjugate pairs $(00 \cdot 2)$-$(00 \cdot 4)$ and $(20 \cdot 3)$-$(20 \cdot 5)$ in the 15-wt%-Nb sample of Fig. 4.]

The Mössbauer results show that the inelastic portion of the diffuse scattering is centered within experimental error at the exact ω positions, while the elastic portion is displaced. In general, as both the diffraction angle and the Nb concentration increase, the inelastic fraction of the diffuse scattering increases with respect to the elastic.

The ω diffuse x-ray scattering at the bcc Bragg position does not increase with increasing order but remains reasonably constant. This implies that there is little long-ranged lattice distortion due to ω-particle formation. Such distortion would produce Huang scattering which would increase roughly as the square of the diffraction vector.

There are two general approaches to describe the structure of the ω phase. In one, we think in terms of isolated ω particles imbedded in a bcc matrix. In the other, we consider the ω phase to be generated by a phonon like distortion. Both approaches have in common that they require strong correlations between ω atom displacements and the surrounding bcc structure. In addition, the wave model generates, for particles longer than a wavelength, a correlation between ω domains. Borie's[12] description seems to be somewhat of a link between both extremes.

Consider first an isolated particle description neglecting any correlation between different ω particles. The ω phase can be described by a hexagonal unit cell containing three atoms located at $(0,0,0)$ and $\pm(\frac{1}{3}, \frac{2}{3}, \frac{1}{3}+U)$ stacked in $ABCA\ldots$ sequence. The hexagonal C axis is parallel to $\langle 111 \rangle_\beta$ and the A-A distance is half the body diagonal (near-neighbor distance) in the cubic unit cell. U is a fraction of this distance. For $U=0$ the structure is cubic. When $U=\frac{1}{6}$ the B and C layers coincide and the ω structure is hexagonal, which we refer to as the full or ideal ω phase. For $0<U<\frac{1}{6}$ the ω lattice has trigonal symmetry. ω particles may be oriented along the four equivalent $[111]_\beta$ directions, which are referred to as variants. Furthermore, there is no *a priori* preference as to which layer is chosen as A (i.e., the fixed layer). The structures resulting from these three choices of fixed planes are called subvariants. The structure factor of the ω unit cell which depends on U can easily be calculated. The structure factors indicated on the ω indices shown in Fig. 7 correspond to full ω phase. Note that along a given layer line, reflections with $H-H' = 3N$ always have the same F^2 independent of U value, i.e., $F^2(20 \cdot 3) = F^2(\bar{1}0 \cdot 3)$, $F^2(00 \cdot 4) = F^2(\bar{3}0 \cdot 4)$, etc.

For a given U value, the ratio of F_ω^2 of any two reflections can be readily calculated. Conversely, a U value may be obtained from the experimental ratio of intensity of two reflections. Figure 14 is a plot of the U parameter for Zr-Nb crystals obtained from the intensity ratio of two ω reflections. For self-consistency, the ratio of peak intensity above the background of $(00 \cdot 2)$ and $(00 \cdot 5)$ are used for all compositions. It is interesting to notice that the U parameters versus composition form two distinct slopes, again suggesting two different regimes of ω structures, with boundary between 15- and 20-wt% Nb. We would have preferred to calculate the parameter from the intensities of the $(10 \cdot 3)$ and $(\bar{1}0 \cdot 3)$ reflections because the two reflections correspond to the same d spacing and therefore any errors involving geometric effects, resolution volume as well as Debye-Waller and static displacement factors affect both in the same manner and are eliminated by taking the intensity ratios. Unfortunately, $(10 \cdot 3)$ is too weak to be measured in the 20- and 30-wt% crystals, but can be obtained from the 8-, 12-, and 15-wt% samples. These U values obtained are about 0.015 higher than those shown in Fig. 14 from $(00 \cdot 2)$ and $(00 \cdot 5)$. The difference indicates some internal discrepancy in the model, which may be caused by Debye-Waller or static displacement factors, which affect $(00 \cdot 5)$ more than $(00 \cdot 2)$. It is an interesting point that the U parameter of the 20-wt% crystal determined from integrated intensity measurements of bcc reflections

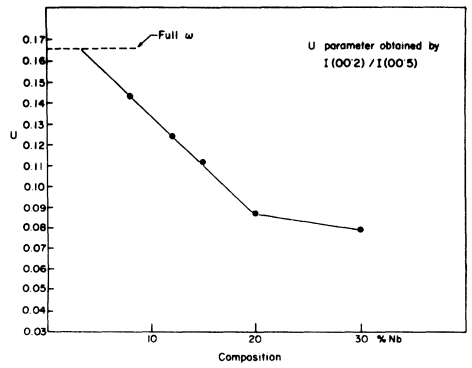

FIG. 14. U parameter as obtained from the ratio of the diffuse ω reflections (00.2) and (00.5) vs composition.

by Keating and LaPlaca[8] is about 0.01 higher than the one shown in Fig. 14.

Our results for the 8-wt%-Nb sample show, contrary to electron microscopy results,[19] that this alloy does not have the sixfold symmetry of the full ω phase. This is readily evident in Fig. 2 since sixfold symmetry would require $(10\cdot 3)$ and $(\bar{1}0\cdot 3)$ to be equal whereas they are in the ratio of 2:3.

Although this particle model may be able to describe the intensities of the ω reflections fairly well, it does not predict any peak shifts at all. Borie *et al.*[12] proposed an *ad hoc* model, which gave a reasonable fit to the intensities and the peak shifts. The crystal was considered to be entirely in the ω phase and the variables were the size and sequence of the three ω subvariants. In the stacking sequence $ABCA\ldots$ they call domains with fixed A, B, or C planes subvariants ω_1, ω_2, and ω_3, respectively. Now they could reproduce the right sign of the ω peak shifts from the exact hexagonal positions only if ω_1 was followed by ω_3 and ω_3 by ω_2. The domains were separated by a defect cell, which they proposed might be a growth fault. This model, however, fails to predict the diffuse scattering that is observed under the bcc reflections.

Much of the interest in the ω phase was generated because of its apparent relation to the more fundamental instability of the bcc lattice with respect to hcp. It is found that the bcc lattice is, in general, soft with respect to longitudinal phonons propagating in a $\langle 111\rangle$ direction with wavelengths $3d_{222}$. (The phonon dispersion has a pronounced minimum at this or a slightly shorter wavelength.) A static longitudinal wave of this precise wavelength would transform bcc into ω. Thus, the suggestion that the $\beta \rightarrow \omega$ transition could be related to some kind of mode softening. The wave model was first proposed by DeFontaine[18] and has recently been worked out and promulgated with thermodynamic arguments by Cook.[21]

If a static sinusoidal modulation is superimposed on a lattice, "phonon sidebands" will arise symmetrically on either side of the reciprocal-lattice points. Let us assume a modulation of the form

$$U = (2U_0/\sqrt{3})\sin(k_\omega x)\,,$$

with $k_\omega = 2\pi/3d_{222}$ and let the nodes of the sine coincide with $(111)_\beta$ planes. This static wave then transforms the bcc structure into ω with U_0 as the displacive parameter discussed above. The sidebands are located exactly at the hexagonal ω-phase positions.

If the observed ω diffuse reflections are centered off the hexagonal lattice and shifted away from the Bragg reflections, it must be assumed the the wavelength of the modulation is slightly shorter than $3d_{222}$. That means

$$U = (2U_0/\sqrt{3})\sin[(k_\omega + \Delta k)x]\,.$$

Because of the mismatch of lattice spacing and wavelength of the distortion there will be no perfect ω structure. The displacements U of the different planes will depend on their position in space as well as on the amplitude of the wave. If the mismatch is small enough, however, there will still be regions of good match, i.e., almost perfect ω structure followed by regions of mismatch and vice versa. If we start in a region of good match which is, let's assume of the ω_1 type (fixed A planes), and proceed in space, it can be easily shown that the next region of good match has to be of the ω_3 type and the next ω_2. Thus, this modulation generates a strong correlation between domains and is exactly the sequence Borie *et al.* empirically found necessary to produce the correct sense of the peak shifts. If Δk is negative (i.e., the wave vector is shorter than the exact ω value), then the sequencing of the subvariants is incorrect. The wave structure and Borie's model, although similar, are not the same. Borie's model proposes domains with a constant U parameter which are separated by defective cells. In the wave model the U parameter varies continuously and the border between domains is diffuse rather than abrupt.

We recall from Sec. III that the structure factors of the ω reflections are strongly dependent on the U parameters. Now we have to ask whether it is possible to reproduce the appropriate structure factors and intensity ratios when the U parameter is no longer constant.

In order to test this we did some computer calculations using various models. We calculated the geometrical structure factor of ω particles using modulations

$$U = (2U_0/\sqrt{3})\sin[(k_\omega + \Delta k)x]\,,$$

and

$$U = (2U/\sqrt{3})\cos(\Delta k x)\sin(k_\omega x)\,.$$

The length of the particle was determined by setting a barrier B so that the boundaries were given by $B \lesssim \cos(\Delta k x_B)$ (according to one of Cook's models a minimum amplitude is needed for the formation of a stable ω structure). The variation of the structure factor along $\langle 00\cdot l\rangle$ was calculated for various values of U and B both for an independent particle and particles randomly arranged within the confines of a bcc lattice. The results are summarized as follows: (i) The peak shifts

are not consistent in all the models. It seems that the observed peak shifts are generated by correlations between different particles rather than by correlations between displacements within one particle (as Cook pointed out). (ii) The ratio $I_{00\cdot1}/I_{00\cdot2}$ is not very much dependent on B and U or on the different models. (iii) $I_{00\cdot4}$ (and with it $I_{00\cdot4}/I_{00\cdot2}$) depends strongly on U and B. For $B \gtrsim 0.8$ the results are very similar to those using a constant U parameter. $I_{00\cdot4}$ approaches zero for $U \approx \frac{1}{12}$, i.e., displacements halfway to full ω phase.

The inconsistency between the observed peaks shifts and the wave model can be resolved in a qualitative way. If we postulate that the lattice spacing in the $\langle 111 \rangle$ direction for an ω particle is somewhat larger than the corresponding spacing in the matrix (a Bain strain) the ω reflections would be shifted to lower angles. If this shift is large enough it could dominate the phononlike shifts and all diffuse peaks would shift towards a lower angle. The shift due to the Bain strain which increases proportional to k would be least for $(00\cdot1)$ and, in fact, this is the only diffuse reflection shifted towards higher k values consistent with the phonon model. Our quantitative results are consistent with this picture, but experimental errors in peak position determinations are too large to draw more quantitative conclusions.

The diffuse intensity around the Bragg peaks is unusual in its constancy irrespective of order of reflection. The simplest interpretation would be that of particle size broadening. An independent particle of finite size would have an interference function which would be periodic in k space. All of the ω variants can contribute scattering at the bcc positions, so that directionality in the individual contributions would tend to be averaged out giving more or less circular contours at these points consistent with observation (see Figs. 2–6).

One of the more intriguing aspects of the present work is the interpretation of the Mössbauer data. The data show that the diffuse ω scattering has both elastic and inelastic portions, and that the centroids of the two types of scattering are not in the same place in k space. The measurement does not allow the determination of energy spectrum of the inelastic scattering. The division between elastic and inelastic is related to the Mössbauer resonance width. All scattered energy shifted from the primary γ ray by more than 2×10^{-8} eV is considered inelastic.

From a simple uncertainty principle argument, one can assign a characteristic time of 10^{-7} sec or shorter to the scattering entity producing the inelastic contribution. This clearly implies a dynamic situation in which small domains within the crystal fluctuate between bcc and ω-like regions. The characteristic times are very much longer than phonon periods and would be quasistatic entities from an x-ray diffraction point of view.

Let us assume that the lowest-energy ω-phase distortion corresponds to a k vector not commensurate with the lattice. Cook[21] has presented thermodynamic arguments supporting this contention. Clearly the experimental results show the diffuse scattering displaced by k_m which is greater than k_ω [at least for the $(00\cdot2)$ and $(00\cdot4)$ reflections]. With this assumption, we can get some feeling for why the inelastic portion is centered at k_ω (the exact ω positions) while the elastic fraction is displaced. The inelastic scattering which reflects short characteristic times is no doubt associated with ω fluctuations which are not only short lived in the time domain, but also are not extended in space. These short ranged fluctuations will have ill-defined k values since the length of the particle is the order of the wavelength. The assumption that k_m wave vectors are more energetically favored than k_ω will apply when k is reasonably well defined. For the short ranged particles, this is not the case so that fluctuations of effective wave vectors larger or smaller than k_ω are equally likely and the scattering centers at the ω positions. In other words, when the ω "particle" is so small, fluctuations to the ω phase (B and C planes collapsing) are as likely as fluctuations to the anti-ω (B and C planes moving toward the fixed A plane) and the scattering centers at the ω position. Admittedly, this is speculative, but it is consistent with the stable fluctuation wave vector. These arguments have been presented in some detail in a series of papers by Cook.[21]

V. SUMMARY AND CONCLUSIONS

We have measured the x-ray and Mössbauer diffuse scattering of a series of Zr-Nb alloys from 8- to 30-wt% Nb. Above 15-wt% Nb the ω-phase scattering is quite diffuse and the Mössbauer measurements show a substantial fraction of inelastic component (energy shift greater than $\approx 2 \times 10^{-8}$ eV). Substantial diffuse scattering is observed in the vicinity of the bcc reflections as well as around the hexagonal ω-phase positions. The former scattering is centered about the nominal bcc reciprocal-lattice points, and is nearly constant in intensity for all points. The scattering about the hexagonal ω points is generally displaced towards lower angles. The displacement is consistent with the superposition of two effects. One a phononlike distortion with a wave vector k_m somewhat larger than k_ω (the exact hexagonal value) and a Bain type of lattice expansion of the ω-like particle.

The elastic Mössbauer diffuse scattering is centered at the displaced ω positions while the inelastic portion is at the exact ω positions.

A general qualitative view of the bcc to ω transformation is as follows: In the metastable athermal regime (i.e., samples quenched from 1000 °C) and measured at room temperature and below, local time-dependent fluctuations occur in which groups of atoms arrange themselves into ω-like regions. The size and time dependence is strongly composition dependent. At 15-wt% Nb and lower these regions are quite large and long lived. One can consider the ω regions to approach closely crystalline trigonal particles, especially for the 8-wt% specimen.

For the 20- and 30-wt% samples the domains of ω fluctuations are quite small (several bcc unit cells in extent). There is a spectrum of characteristic times (a substantial fraction $> 10^{-7}$ sec) and sizes associated with the excursions towards the ω phase from the bcc. A given region of crystal will fluctuate in and out of an ω-like regime. The entire crystal will have a statistically constant amount in ω-like regions at any one temperature and will change reversibly as the temperature is varied.

We do not have a detailed structural model to explain the varied diffraction effects from these series of Zr-Nb alloys. We have presented in this paper some unusual scattering effects from these alloys which are still to be quantitatively explained.

ACKNOWLEDGMENTS

We are indebted to Professor S. Sass for supplying us with the Zr-Nb samples and for many helpful discussions. The work was supported by the NSF through the Materials Science Center at Cornell University. One of us (H.S.) is particularly indebted to the Max Kade Foundation, N.Y., for supporting his stay at Cornell through a Max Kade postdoctoral research exchange grant.

---

*Present address: Engineering Research Center, Western Electric Co., P. O. Box 900, Princeton, N. J. 08540.

†Present address: Experimental Physik I, Technische Hochschule Darmstadt, 61 Darmstadt, W. Germany.

[1]J. M. Silcock, M. H. Davies, H. K. Hardy, *Symposium on the Mechanism of Phase Transformations in Metals* (Institute of Metals, London, 1955), pp. 93–104.

[2]B. S. Hickman, J. Mater. Sci. 4, 554 (1969).

[3]D. J. Cometto, G. L. Houze, Jr., and R. F. Hehemann, Trans. AIME 233, 30 (1965).

[4]D. Stewart, B. A. Hatt, and J. A. Roberts, Br. J. Appl. Phys. 16, 1081 (1965).

[5]B. A. Hatt and J. A. Roberts, Acta Metall. 8, 575 (1960).

[6]C. W. Dawson and S. L. Sass, Metall. Trans. 1, 2225 (1970).

[7]S. L. Sass, J. Less-Common Met. 28, 157 (1972).

[8]D. T. Keating and S. J. LaPlaca, J. Phys. Chem. Solids 35, 879 (1974).

[9]S. C. Moss, D. T. Keating, and J. D. Axe, Bull. Am. Phys. Soc. 18, 313 (1973).

[10]B. W. Batterman, G. Maracci, A. Merlini, and S. Pace, Phys. Rev. Lett. 31, 27 (1973).

[11]S. C. Moss, D. T. Keating, J. D. Axe, in *Phase Transformations*, edited by L. E. Cross, (Pergamon, New York, 1973), p. 179.

[12]B. Borie, S. L. Sass, and A. Andreassen, Acta. Crystallogr. A 29, 585 (1973); 29, 594 (1973).

[13]Crystal preparation procedure: (a) polish with 600, 800, 1200, 2400, 3200 SiC powders; (b) polish with alumina water solution (0.3 μm→ 0.05 μm); (c) etching with H_2O:HNO_3:HF solution.

[14]For a general description of the technique refer to B. E. Warren, *X-Ray Diffraction* (Addison-Wesley, Boston, Mass., 1969), Chap. 11.

[15]B. E. Warren, J. Appl. Phys. 25, 814 (1954); D. R. Chipman, Rev. Sci. Instrum. 27, 164 (1956).

[16]B. W. Batterman, D. R. Chipman, and J. J. DeMarco, Phys. Rev. 122, 68 (1961).

[17]C. Ghezzi, A. Merlini, S. Pace, Nuovo Cimento B 64, 103 (1969).

[18]D. DeFontaine, Acta. Metall. 18, 275 (1970).

[19]S. L. Sass and B. Borie, J. Appl. Crystallogr. 5, 236 (1972).

[20]C. Goasdove, P. S. Ho, S. L. Sass, Acta. Metall. 20, 725 (1972)

[21]H. E. Cook, Acta. Metall. 22, 239 (1974); 21, 1431 (1973); 21, 1445 (1974).

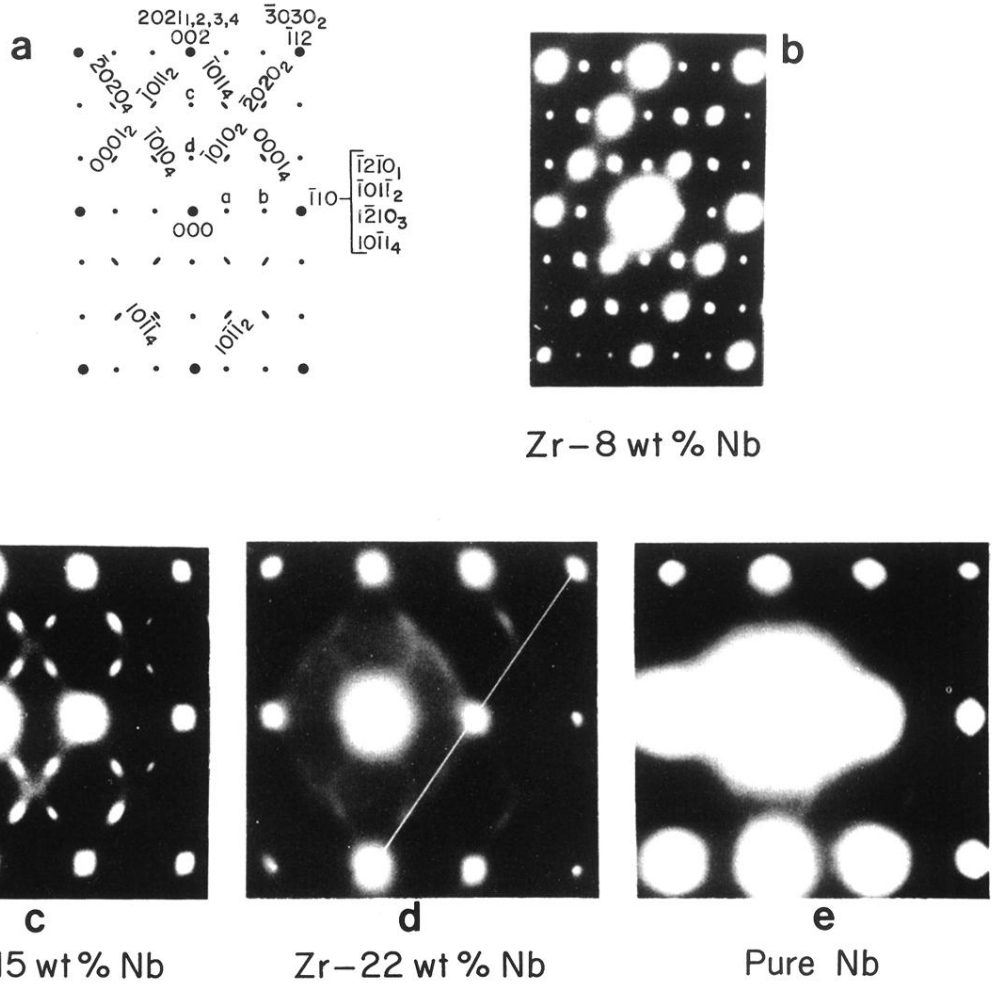

FIG. 1. Comparison of (110) electron diffraction patterns of several Zr-Nb alloys (from Sass, Ref. 7). (a) Schematic diffraction pattern giving indices of the reflections shown in (b)–(e). The subscripts refer to orientations of the ω phase with respect to the four different [111] directions (variants). (b) 8-wt% Nb, (c) 15-wt% Nb, (d) 22-wt% Nb, (e) pure Nb.